Modeling, Control, and Harmonic Mitigation of a Hybrid PV Generation System Interconnected through Bipolar LCC-HVDC Transmission

Ramy Adel Younis[1]

ABSTRACT

Abstract— *This paper presents the modeling, control, and performance evaluation of a hybrid photovoltaic (PV) generation system interconnected with the grid through a bipolar Line Commutated Converter High Voltage Direct Current (LCC-HVDC) transmission network. The system, inspired by the Egypt–Saudi Arabia interconnection project, was developed in MATLAB/Simulink to emulate long-distance renewable integration. A 10 MW PV plant was modeled with Maximum Power Point Tracking (MPPT) and interfaced through DC–DC boost converters to the LCC rectifier. The converters were configured in a 12-pulse topology with coordinated control of firing and extinction angles. Simulation results demonstrated stable active power transfer of approximately 1300 MW with DC current around 1350 A during steady-state operation. Under irradiance variation from 1000 W/m² to 500 W/mhe PV output power decreased by 6.5%, verifying system sensitivity to environmental variations. Harmonic analysis revealed that without filtering, the rectifier-side AC bus voltage exhibited a Total Harmonic Distortion (THD) of 13.94%, which significantly exceeds IEEE Std. 519 limits. By implementing tuned and damped passive filters, the THD was reduced to 0.93%, restoring sinusoidal voltage waveforms and improving power quality. The study demonstrates that coordinated firing/extinction angle control and optimized filter design are crucial for reliable renewable–HVDC integration, ensuring both compliance with international standards and efficient long-distance power transfer.*

Keywords Photovoltaic generation, Line Commutated Converter (LCC), High Voltage Direct Current (HVDC), Bipolar HVDC transmission, MPPT control and Total Harmonic Distortion THD, Power quality improvement.

I.INTRODUCTION

The global energy landscape is undergoing a profound transformation driven by the urgent need to reduce carbon emissions, diversify energy sources, and ensure long-term sustainability. Renewable energy resources (RES), particularly photovoltaic (PV) and wind power, are increasingly deployed worldwide due to their abundance and declining costs [1], [2]. However, their variability and intermittency present significant challenges for maintaining grid stability and power quality, especially when integrated at large scale. Addressing these issues requires advanced transmission technologies and robust control strategies capable of ensuring reliable renewable integration.

High Voltage Direct Current (HVDC) transmission has emerged as a preferred technology for interconnecting remote renewable sources and linking asynchronous power systems across long distances. Compared with alternating current (AC) transmission, HVDC provides lower transmission losses, higher stability margins, and the ability to transfer bulk power between systems operating at different frequencies [3]. Among HVDC technologies, the **Line Commutated Converter (LCC-HVDC)** remains the dominant choice for bulk power transfer because of its technological maturity, cost-effectiveness, and proven deployment in projects exceeding several gigawatts [4]. However, LCC-HVDC has inherent technical challenges such as reactive power consumption, sensitivity to commutation failures, and the generation of harmonic distortion [5], [6]. These issues necessitate advanced control strategies for the firing (α) and extinction (γ) angles, as well as effective harmonic mitigation through appropriately designed filters.

In recent years, several research efforts have focused on renewable–HVDC integration. Wang et al. [7] investigated the dynamic performance of renewable energy integrated HVDC systems and highlighted stability challenges under weak grid conditions. Shi et al. [8] proposed multi-objective optimization for AC filter design in HVDC systems, achieving significant THD reduction. Alamoudi and Abdelaleem [9] analyzed the role of firing and extinction angles in regulating power transfer of LCC-HVDC, demonstrating their impact on both power flow and converter stability. On the renewable side, Ahmed et

al. [10] modeled hybrid PV–wind generation systems with MPPT control, while Younis et al. [11], showed the potential of optimization-based approaches for improving system efficiency and cost-effectiveness. These studies collectively demonstrate the importance of hybrid renewable integration but also highlight the need for transmission-level investigations where hybrid farms are interconnected via HVDC systems. Mao et al. [12] examined hybridization strategies to enhance energy reliability. Liang et al. [13] provided a comprehensive review of control issues in LCC-HVDC with embedded renewables, emphasizing the critical need for coordinated angle control and reactive power compensation.

Despite these contributions, many existing studies treat PV, wind, and HVDC independently or in simplified frameworks. Limited work has been conducted on **comprehensive hybrid renewable systems modeled with realistic parameters, integrated through a bipolar LCC-HVDC link, and controlled under different firing and extinction angle scenarios**. Furthermore, the issue of harmonic mitigation remains critical, as unfiltered systems can exceed IEEE THD limits and compromise grid stability. Passive filters remain a widely adopted solution due to their simplicity and effectiveness, but their design and placement require careful consideration to suppress dominant harmonics such as the 5th, 7th, 11th, and 13th orders [14].

Motivated by the **Egypt–Saudi Arabia interconnection project**, a large-scale 3000 MW HVDC initiative designed to link the 50 Hz Egyptian grid with the 60 Hz Saudi Arabian grid [15], this paper develops a detailed MATLAB/Simulink model of a hybrid PV integrated to grid with -HVDC system. The model represents a **10 MW PV farm integrated through a 12-pulse LCC-HVDC link**, incorporating MPPT for maximum solar utilization and passive filters for harmonic suppression. The study evaluates system performance under scenarios of irradiance variation and converter angle control, highlighting the influence of firing and extinction angle adjustments on power transfer and power quality.

The novelty of this work lies in combining **hybrid renewable modeling, LCC-HVDC transmission, angle-based converter control, and passive filter-based harmonic mitigation** into a single comprehensive simulation framework table 1 shows the comparison with relative studies. This approach not only reflects real-world cross-border energy integration projects but also provides valuable insights into improving the reliability and efficiency of renewable energy transmission over long distances.

Table 1 Comparative Review of Related Work on Renewable Integration and LCC-HVDC Systems

Reference	Sources Modeled	Control Approach	HVDC Focus	Limitations	Relevance to Present Work
Wang et al., 2021 [7]	Wind + Grid	Dynamic stability analysis	LCC-HVDC	Focused on commutation failures; no PV modeling	Provides insights into weak-grid interaction
Shi et al., 2023 [8]	Grid only	Multi-objective optimization (MOEA/D)	AC filter design in HVDC	No renewable sources considered	Supports filter methodology
Alamoudi 2022 [9]	Grid only	Firing & extinction angle variation	LCC-HVDC	Did not model renewable sources or filters	Basis for α–γ control strategies
Ahmed et al., 2020 [10]	PV + Wind	MPPT control, hybrid farm modeling	No HVDC	Stand-alone hybrid system	Provides foundation for renewable farm modeling
Mao et al., 2023 [11]	PV + Wind	Seasonal/dynamic simulation	No HVDC	Focused only on generation-side	Highlights hybridization benefits
Liang et al., 2024 [12]	PV + Wind + Grid	Literature review	LCC-HVDC	Review only; no simulation	Identifies research gaps in HVDC + RES
Younis et al., 2022 [13]	PV + Wind + Storage	Metaheuristic optimization (NGO, RTLBO, etc.)	Stand-alone microgrid	Techno-economic only; no HVDC	Links optimization with hybrid RES

This work (2025)	PV farm + Grid (Egypt–KSA)	MPPT + firing angle (α) & extinction angle (γ) control; passive filter design	LCC-HVDC (12-pulse, bipolar)	No wind or cost analysis	Novel integration of PV farm with LCC-HVDC and harmonic mitigation

Recent literature has addressed several aspects of renewable integration into HVDC systems, yet important gaps remain. Jin et al. [15] proposed additional frequency control strategies to improve the adaptability of asynchronous LCC-HVDC links, but their work did not consider the presence of renewable sources or harmonic effects. Similarly, Peihong et al. [16] investigated harmonic coupling under geomagnetic storms, focusing on extreme disturbances rather than routine converter–filter interactions in renewable-based grids. In harmonic mitigation, Wang and Wang [17] designed multi-band band-stop filters for MMC-HVDC, and Mehmood et al. [20] introduced double-damped tuned filters for conventional HVDC; however, both approaches are hardware-intensive and were not validated within hybrid renewable environments. On the renewable side, Li et al. [18] explored frequency support for offshore wind farms using VSC-HVDC, while Ismail Hossain et al. [23] analyzed PV and wind integration into MMC-HVDC; these studies are insightful but rely on VSC technology, which differs significantly from the more established LCC deployments in bulk transmission. Likewise, Wang et al. [19] focused on multi-terminal HVDC with renewables, and Zeng and Wang [24] examined resonance suppression in MMC-HVDC systems—both valuable but centered on MMC rather than LCC configurations. At the system level, Liu et al. [21] proposed distributed emergency frequency control, and a recent review [22] emphasized HVDC's role in weak grids, yet neither addressed detailed PV modeling or coordinated angle control in LCC-HVDC.

In contrast, the present work develops a comprehensive MATLAB/Simulink model of a hybrid PV farm integrated through a 12-pulse LCC-HVDC system. Unlike prior studies, this work explicitly combines PV array modeling with MPPT, coordinated firing and extinction angle control, and passive filter design for THD suppression. This integrated approach not only addresses renewable variability and harmonic distortion but also aligns with the real-world Egypt–Saudi Arabia interconnection project, thereby offering both academic novelty and practical relevance.

.

The main contributions of this work are: (i) development of a detailed PV integrated to grid with –LCC-HVDC simulation model; (ii) implementation of coordinated firing angle and extinction angle control strategies; and (iii) assessment of harmonic performance to demonstrate the feasibility and operational benefits of integrating large-scale renewable generation through LCC-HVDC transmission links.

The remainder of this paper is structured as follows. **Section II** provides an overview of renewable energy modeling, covering PV and wind technologies with their electrical characteristics. **Section III** introduces HVDC transmission technology, including LCC fundamentals, converter station structure, and filter requirements. **Section IV** presents the system modeling in MATLAB/Simulink, covering PV arrays, wind turbine models, and the LCC-HVDC link. **Section V** describes the LCC converter control, focusing on firing angle, extinction angle, and passive filter design. **Section VI** presents simulation results under various irradiance and control scenarios, with discussion of system performance and harmonic suppression. Finally, **Section VII** concludes the paper with key findings and outlines directions for future research.

[1] Electrical Power and Machines Engineering Department, The Higher Institute of Engineering at El-Shorouk City, El-Shorouk Academy, Cairo, 11837, Egypt.

[2] Author Affiliation

* Ramy Adel younis, r.adel@sha.edu.eg

II. MATERIALS AND METHODS

A. System description

The proposed system as described in figure 1 comprises a large-scale photovoltaic (PV) generation plant integrated with a bipolar Line Commutated Converter-based High Voltage Direct Current (LCC-HVDC) transmission link. This configuration is designed to emulate long-distance, high-power renewable energy transfer, inspired by real-world interconnection projects such as the Egypt–Saudi Arabia HVDC initiative.

The PV generation system consists of ten identical units, each rated at 1 MW, resulting in a total installed capacity of 10 MW. Each unit includes detailed PV array modeling with Maximum Power Point Tracking (MPPT) control based on perturb and observe algorithms, and is interfaced through DC-DC boost converters. The combined output from the PV arrays is directed to the LCC rectifier station.

The rectifier and inverter stations are modeled using two six-pulse converters connected in series to form a twelve-pulse bridge topology. The converters are energized through phase-shifted transformer configurations (Y/Y and Y/Δ), which enable harmonic cancellation of lower-order harmonics (notably the 5th and 7th). The DC link spans a simulated length of 100 km, representing realistic overhead line and cable segments in HVDC infrastructure.

Reactive power compensation and harmonic mitigation are achieved through the design and implementation of passive AC filters on both sides of the converter stations. These filters are tuned to attenuate dominant harmonics and reduce Total Harmonic Distortion (THD), ensuring compliance with grid code standards.

The entire system is developed and simulated in MATLAB/Simulink. Multiple case studies are conducted under varying irradiance conditions and firing/extinction angle configurations to assess power quality, voltage waveform purity, and control responsiveness. The coordinated control strategy incorporates both open-loop and closed-loop firing angle regulation, including Constant Current Control (CCC) and minimum angle enforcement for commutation security.

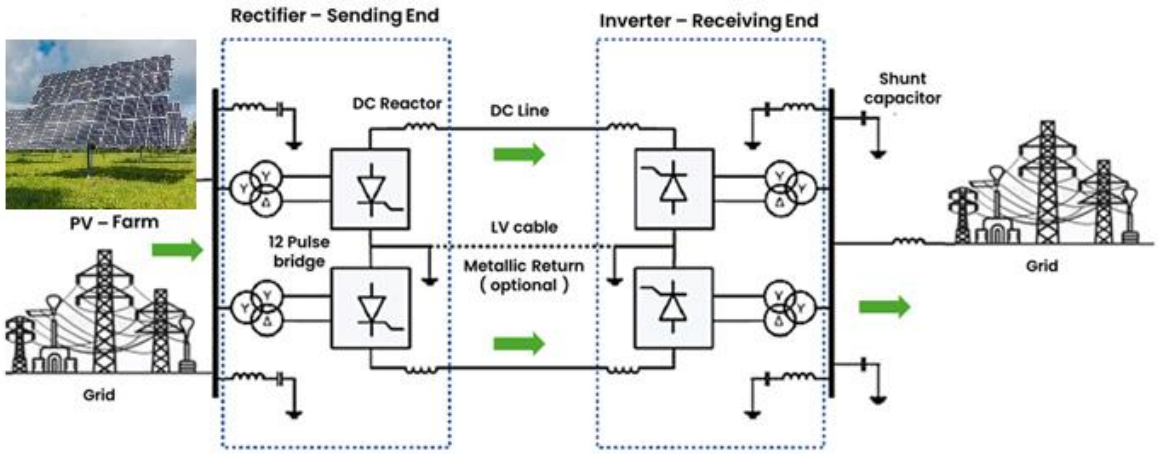

Figure 1 : Schematic diagram for the proposed system hybrid PV power system

B. Modelling and Methodology

1- Ideal One Diode Model:

Figure 2 is the most simplified form of an ideal PV cell through which the output voltage and current relations comes out to be as following equations :

$$I = I_{ph} - I_D \quad (1)$$

$$I_D = I_o\left(e^{\frac{V}{N_s VT}} - 1\right) \quad (2)$$

$$VT = \frac{NKT}{q} \quad (3)$$

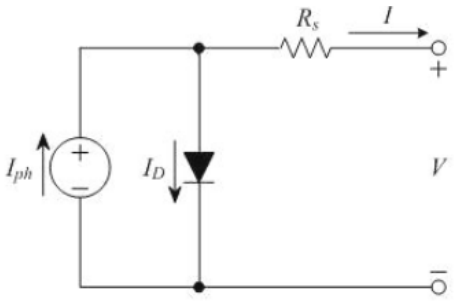

Figure 1 an equivalent circuit of an ideal PV cell

The ideal one-diode model represents the most simplified equivalent circuit of a photovoltaic (PV) cell [11-12], capturing its fundamental electrical behavior. In this model, the PV cell is depicted as a current source connected in parallel with a single ideal diode. The resulting current–voltage (I–V) characteristic equation describes the output current as the difference between the photocurrent generated by incident solar irradiation and the diode's exponential current response governed by the Shockley equation. Despite its simplicity, this model provides an effective first approximation for analyzing PV performance under uniform operating conditions, and it serves as a foundation for developing more refined models that incorporate additional losses and non-linearities.

2- Real Diode Model:

The real diode model extends the ideal representation by incorporating practical losses that affect the performance of a photovoltaic cell [13]. In this configuration, the equivalent circuit consists of a current source in parallel with a diode, complemented by two resistive components: a series resistance (Rs) and a shunt resistance (Rsh).

The series resistance accounts for the voltage drop due to internal cell material resistance and contacts, which causes a reduction in the fill factor and output power under load. The shunt resistance models leakage currents across the p-n junction and represents imperfections in the cell structure, resulting in deviation from ideal behavior, especially under low irradiance conditions. By including these resistive effects, the real diode model provides a more accurate and practical estimation of the I–V characteristics, enabling improved simulation and performance prediction of PV modules under variable environmental and operating conditions.

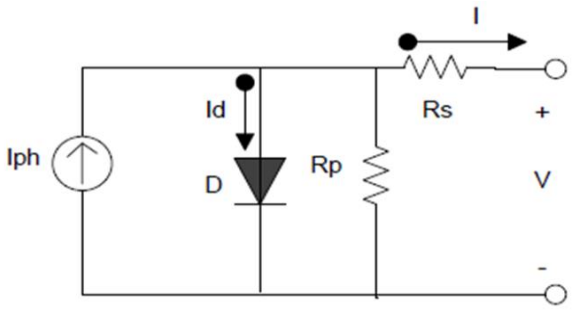

Figure 3 an equivalent circuit of an ideal PV cell

$$I = I_{ph} - I_o\left(e^{\frac{V+IR_s}{n_s VT}} - 1\right) - \frac{V + IR_s}{R_p} \quad (4)$$

3. Control basics for a two-terminal DC link

The single line diagrams in figure (4a) shows a HVDC link

and an equivalent circuit is shown in figure (4b) [3].

A two terminal DC link is shown in figure (4) with a rectifier and an inverter. The DC system is represented by an inductance L and a line resistance R; the value of the inductance L comprises the smoothing reactor(s), DC line inductance whereas the value of R includes the resistances of the smoothing reactor(s) and the resistance of the DC line etc. Applying Ohm's law, the DC current in the DC link depicted in Figure 4 is given by Eq:

$$I_d = \frac{V_{dr} - V_{di}}{R} \quad (5)$$

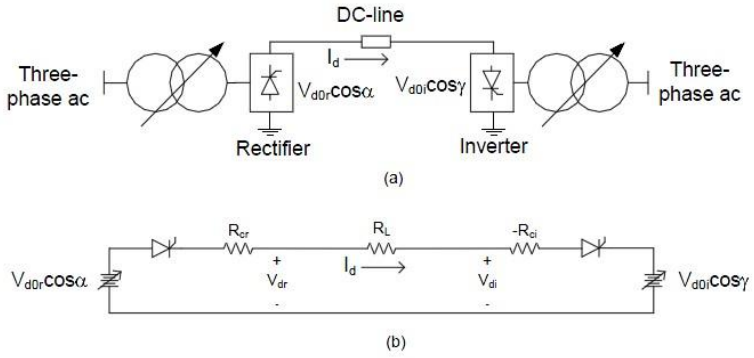

Figure 4 (a) Schematic diagram of a HVDC link (b) Equivalent circuit.

Where: V_{dr}: DC-Voltage output of the rectifier, V_{di}: DC-Voltage output of the inverter, R: The DC line Resistance.

Then, the power at rectifier side of DC link is given by:

$$P_{dr} = V_{dr} * I_{dr} \quad (6)$$

The power at rectifier side of DC link is computed as:

$$P_{di} = V_{di} * I_{di} \quad (7)$$

From converter theory, the relationship V_d-I_d for a rectifier is given by:

$$V_{dr} = V_{dor} \cos \alpha - R_{cr} I_d \quad (8)$$

where R_{cr} and R_{ci} depend on the overlap angles at the rectifier and the inverter respectively. If the overlap angles is zero, their associated voltage drop equal to zero with overlap, R_{cr} equals to $\frac{3X_{cr}I_d}{\pi}$ and Rci equals to $\frac{3X_{ci}I_d}{\pi}$. Id is the DC current and X_{cr} is the commutation reactance (of the HVDC transformer) at the rectifier. X_{ci} is the commutation reactance of the inverter.

V_{dor} = 1.35 V_{Lr} is the maximum DC voltage of rectifier with firing angle $\alpha = 0$. V_{Lr} is the rms value of line input voltage of the rectifier, while V_{doi} =1.35 V_{Li} is the maximum DC voltage for the inverter with γ=0 and V_{Li} is the rms value of line input voltage of the inverter. Using the equations describing V_{dr} and V_{di} the DC line current is given by either one of two options depending upon the choice of the control mode at the inverter:

The DC output power of the rectifier and inverter equations shows the power transmitted depending on the V_{dor}, V_{doi}, α, γ and the DC current.

$$P_{dr} = V_{dor} I_d \cos(\alpha) - R_{cr} I_d^2 \quad (9)$$

$$P_{di} = V_{doi} I_d \cos(\gamma) - R_{ci} I_d^2 \quad (10)$$

The reactive power is absent inside HVDC link, therefore the using of fixed capacitors and filters at each AC side to supplement the reactive power as mentioned before.

The best choice selects γ =180- α is to educe the voltage drop between output of the rectifier and the input of inverter inside the HVDC link.

4. Design of Filters

AC filters are crucial in High Voltage Direct Current (HVDC) systems to reduce harmonic distortion caused by converter operations. They are passive circuits designed to provide low impedance shunt paths for harmonic currents, ensuring power quality standards. Tuned filters target the 11th and 13th harmonics, while damped filters suppress higher harmonics and provide reactive power support. Modern filter designs include C-type filters, double- and triple-tuned filters, and active AC filters, which may offer more flexible solutions for harmonic compensation in HVDC networks.

In HVDC systems, AC filters are essential components used to mitigate the harmonic distortion generated by the converter operations on the AC side. These filters are typically passive circuits designed to provide low impedance shunt paths for harmonic currents, thereby preventing their propagation into the connected AC network and ensuring compliance with power quality standards. A conventional 12-pulse converter station generates characteristic harmonics at the order of n=±12k, where k is an integer. Therefore, tuned filters are commonly designed for the 11th and 13th harmonics, which are dominant in such systems. These filters are known as single-tuned filters and are composed of passive RLC elements specifically designed to target certain harmonic frequencies. For higher-order harmonics, damped filters—typically tuned around the 23rd harmonic—are employed. These filters not only suppress higher harmonics but also provide reactive power support to the system. Modern filter designs may also include C-type filters, which are more cost-effective and allow for a broader damping range while maintaining good filtering performance. In addition, double- and triple-tuned filters have been introduced to reduce the total number of filter branches required, hence reducing installation space and cost. Although currently passive filters are widely used due to their simplicity and reliability, active AC filters are emerging technologies that may soon provide more flexible and dynamic solutions for harmonic compensation in HVDC networks [14].

- Passive Harmonic Filter Design in HVDC Systems

In high-voltage direct current (HVDC) transmission systems, particularly those based on line-commutated converter (LCC) technology, power electronic switching introduces significant harmonic distortions on the AC side. These

harmonics, if not properly mitigated, can lead to voltage waveform distortion, overheating of equipment, increased losses, malfunction of protective devices, and reduced overall system reliability as show in figure 5.

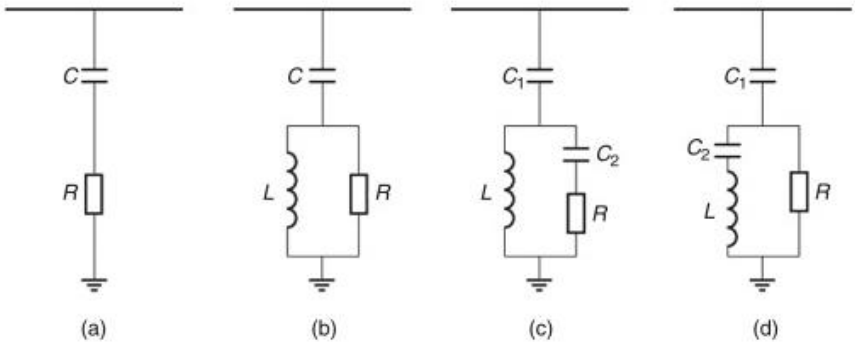

Figure 5: High-pass damped filters: (a) First order; (b) second order; (c) third order; (d) C-type

To address these challenges, passive harmonic filters are widely employed. These filters, constructed using passive elements such as capacitors (C), inductors (L), and resistors (R), are strategically connected to the AC buses of converter stations. Their dual role includes:

- Attenuating specific harmonic frequencies, typically those introduced by the 12-pulse converter operation (e.g., 11th, 13th, 23rd, etc.).
- Providing reactive power compensation, which is essential for the operation of LCC-based HVDC systems that inherently absorb reactive power.

In the CIGRÉ benchmark HVDC model, the total required reactive power per converter station is approximately 625 Mvar. This requirement is distributed among various filtering and compensation components to ensure proper harmonic suppression and system voltage control. The distribution is typically as follows [15]:

- 40% of the reactive power is provided by a second-order high-pass damped filter targeting high-frequency harmonics.
- 40% is provided by a C-type damped filter, which focuses on eliminating low-order harmonics.
- The remaining 20% is supplied by fixed capacitor banks to maintain voltage levels and compensate for system demands.

Each filter type is tuned to a specific harmonic frequency and designed based on key parameters such as system voltage, harmonic order, desired reactive power contribution, and quality factor. The following sections describe in detail the structure, function, and design equations of each filter, following the methodology derived from the CIGRÉ standard.

1- Second-Order High-Pass Damped Filter

This filter is designed to target higher-order harmonics such as the 11th or 13th harmonic as show in figure 6 . It consists of a series capacitor C1, an inductor L1, and a damping resistor R. When tuned to a specific harmonic frequency, the LC branch presents very low impedance at that frequency, diverting harmonic currents away from

the AC network and through the filter. The damping resistor is essential to suppress excessive resonance and improve system stability.

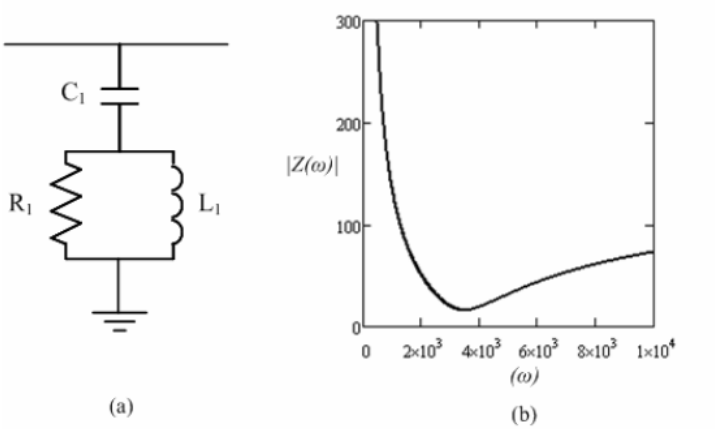

Figure 6 : 2nd order high-pass damped filter: (a) configuration; (b) impedance characteristic

Design Equations:

- Capacitive Reactance:

$$Xc = \frac{V^2}{Q} \qquad (11)$$

- Capacitance:

$$C_1 = \frac{1}{(\omega \times X_C)} \qquad (12)$$

- Inductive Reactance:

$$X_L = \frac{X_C}{h_r^2} \qquad (13)$$

- Inductance:

$$L_1 = \frac{X_L}{\omega} \qquad (14)$$

- The characteristic reactance is

$$Xn = \sqrt{Xl \times Xc} = \sqrt{\frac{L_1}{C_1}} \qquad (15)$$

- Damping Resistance:

$$R_1 = q \times \sqrt{\frac{L_1}{C_1}} \quad (16)$$

Where:h_r is the target harmonic order (e.g., 11),$\omega=2\pi f$ and q is the quality factor.

2-General C-Type Damped Filter

The C-type filter is designed to suppress low-order harmonics such as the 3rd and 5th as show in figure 7. It features minimal losses at the fundamental frequency and strong attenuation at the tuned harmonic frequency. Its topology includes two capacitors C2 , C3 , an inductor L2, and a damping resistor R2. An intermediate design parameter mmm controls the division of capacitance and overall filter shape.

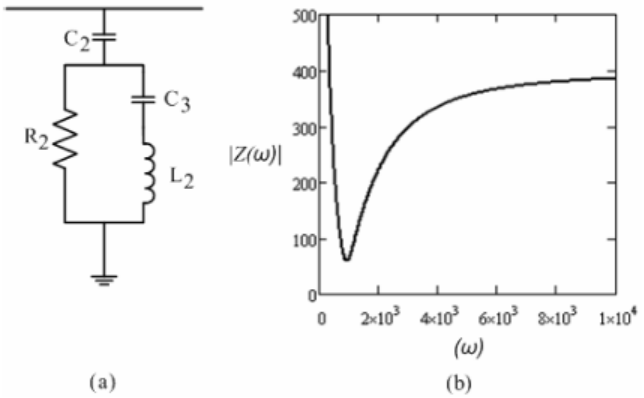

Figure 7: C-type damped filter: (a) configuration; (b) impedance characteristic

Design Equations:

- Capacitive Reactance :

$$X_C = \frac{V^2}{Q} \quad (17)$$

- Capacitance C2 :

$$C_2 = \frac{1}{(\omega \times X_C)} \quad (18)$$

- Capacitance C3 :

$$C_3 = \left(\frac{Q}{(\omega \times V^2)}\right) \times \left(\frac{m}{((m-1)^2 \times h_r^2)}\right) \quad (19)$$

- Inductance L2 :

$$L_2 = \left(\frac{Q}{(\omega \times V^2)}\right) \times \left(\frac{1}{((m-1)^2 \times h_r^2)}\right) \quad (20)$$

- Damping Resistance R2 :

$$R2 = \frac{(q \times V^2)}{(Q \times hr)} \quad (21)$$

III. RESULTS

To validate the performance of the proposed PV–Wind–LCC-HVDC system, several test cases were simulated in MATLAB/Simulink under different operating conditions. The study covered both steady-state and transient scenarios. First, the hybrid system was evaluated under constant irradiance to establish baseline performance. Then, dynamic variations were introduced, including sudden changes in solar irradiance and controlled adjustments of converter firing and extinction angles. Finally, Additional analyses addressed the impact of commutation overlap on voltage waveforms, harmonic distortion assessment without filtering, and harmonic mitigation using passive filters. The following subsections present and discuss each case in detail.

A. Bipolar HVDC Link between Two Grids Steady-state performance

The HVDC system in a Bipolar configuration, showcasing its robust design for efficient and reliable power transmission. The bipolar setup consists of two independent poles, each operating at opposite polarities, ensuring higher power transfer capacity. This configuration not only minimizes transmission losses but also provides system redundancy, as one pole can continue operation if the other fails, ensuring uninterrupted power delivery. This advanced design underscores the HVDC system's adaptability and efficiency in long-distance, high-voltage applications.

The input voltage waveform, the filter exhibits significant improvement in stability and smoothness. The added filtering mechanism effectively mitigates the harmonic distortions previously observed, ensuring a cleaner and more reliable input signal. This enhancement lays the groundwork for optimal rectification performance and improved overall system efficiency.

B. Case I — Steady-state performance (constant irradiance, $\alpha = 20°$, $\gamma = 160°$)

The dynamic response of the modeled hybrid PV–LCC-HVDC transmission system is presented in Figures [8(a)–8(c)]. Figure 8(a) shows the phase voltages at both the rectifier and inverter terminals under steady-state operation. The waveforms demonstrate well-formed sinusoidal profiles with negligible distortion, confirming the effectiveness of the 12-pulse converter configuration and the implemented AC filtering scheme. The inverter side voltages exhibit a stable amplitude synchronized with the receiving grid frequency of 60 Hz, while the rectifier side operates at 50 Hz as defined in the system setup.

Figures 8(b) and 8(c) illustrate the active and reactive power flows at the rectifier and inverter stations, respectively. At the rectifier side (Figure 8(b)), the active power quickly ramps up to approximately 2.3 MW following the initial transient, while the reactive power stabilizes near 1.5 MVAr as the converter establishes continuous conduction. The inverter station response in Figure 8(c) shows the corresponding absorption of active power, with the waveform settling to approximately –2.3 MW, indicating consistent power transfer across the DC link. A slight overshoot is observed during the initial switching period before reaching steady state.

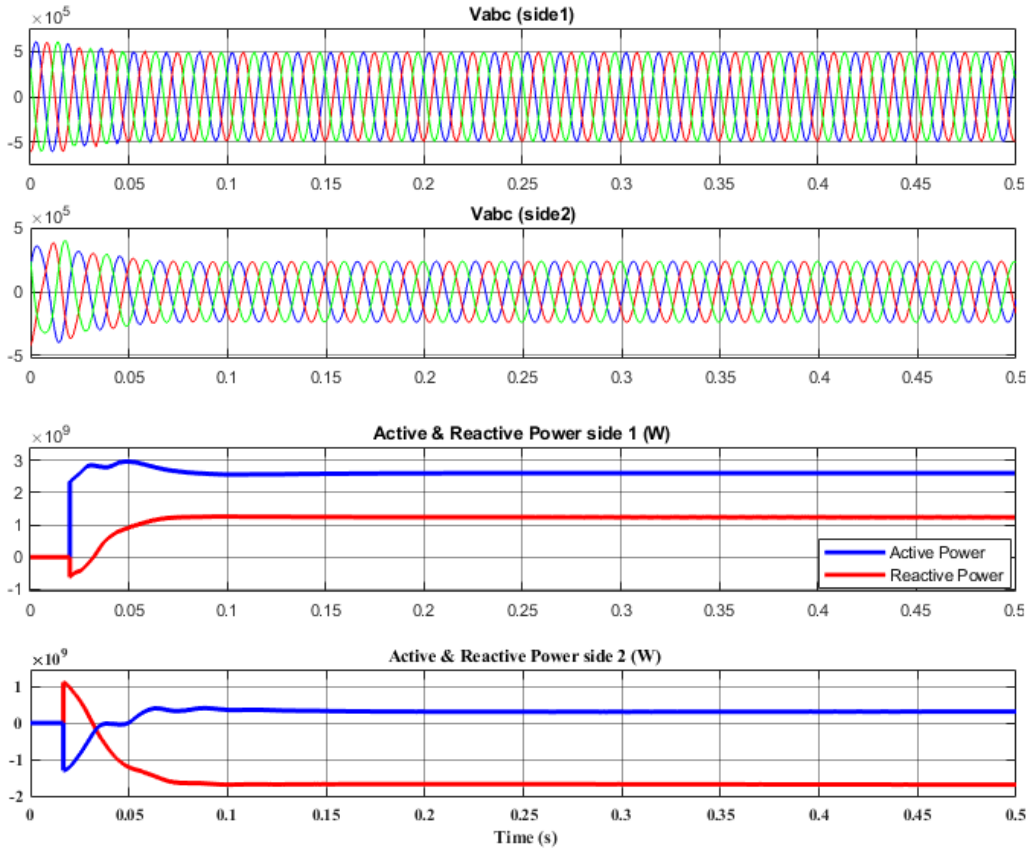

Figure 8 System performance at the rectifier and inverter station (Grid side) (a) Voltage (b)Rectifier side active and reactive power measurement (c) Inverter side active and reactive power measurement.

Figure 9 illustrates the instantaneous DC voltage waveforms at both the sending (rectifier) and receiving (inverter) ends of the LCC-HVDC link at alpha 20 and gamma 160 deg. the rectifier-side voltage (Vdc_rec), which fluctuates around 9×10^5 V with a characteristic ripple caused by the 12-pulse operation. the inverter-side voltage (Vdc_inv), which exhibits a similar ripple but higher average voltage consistent with bipolar operation. The sawtooth pattern in both waveforms is indicative of the switching actions of the thyristor valves and transformer phase-shifting, confirming successful commutation under normal conditions. The ripple amplitude is within acceptable design tolerances, suggesting proper dimensioning of DC reactors and effective HVDC smoothing.

.

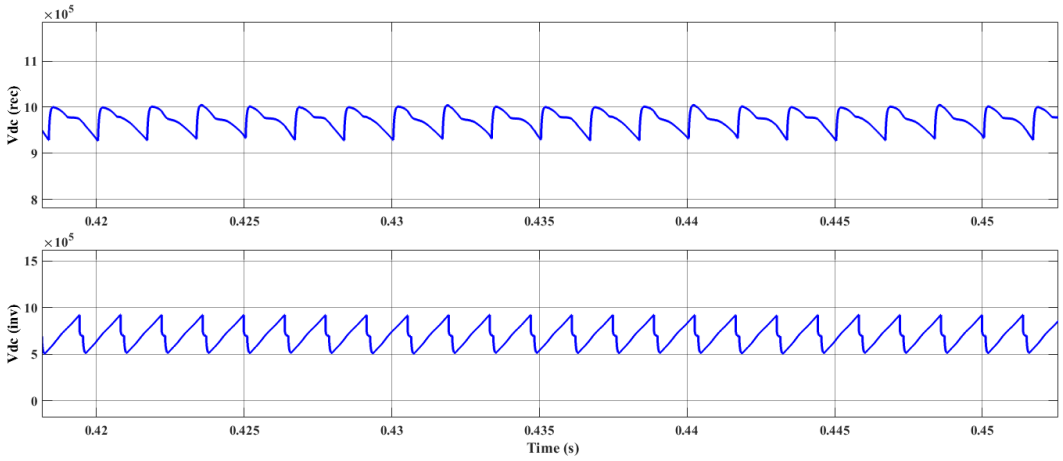

Figure 9 The DC voltage output at alpha 20 and gamma 160 deg.

Figure 10 shows the evolution of total transmitted DC power (Pdc) and DC current (Idc) over time. the power rapidly rises to a steady-state value of approximately 13×10^8 W (1300 MW) within the first 0.06 seconds, after which it remains constant, reflecting the fast dynamic performance of the system and stable MPPT operation at the PV side. the DC current ramping up to approximately 1350 A, after which it saturates. The smooth rise and lack of oscillation in both parameters indicate strong system damping and the absence of resonant conditions. This also confirms that the control systems, particularly for MPPT and HVDC firing/extinction angle adjustment, maintain system integrity during startup.

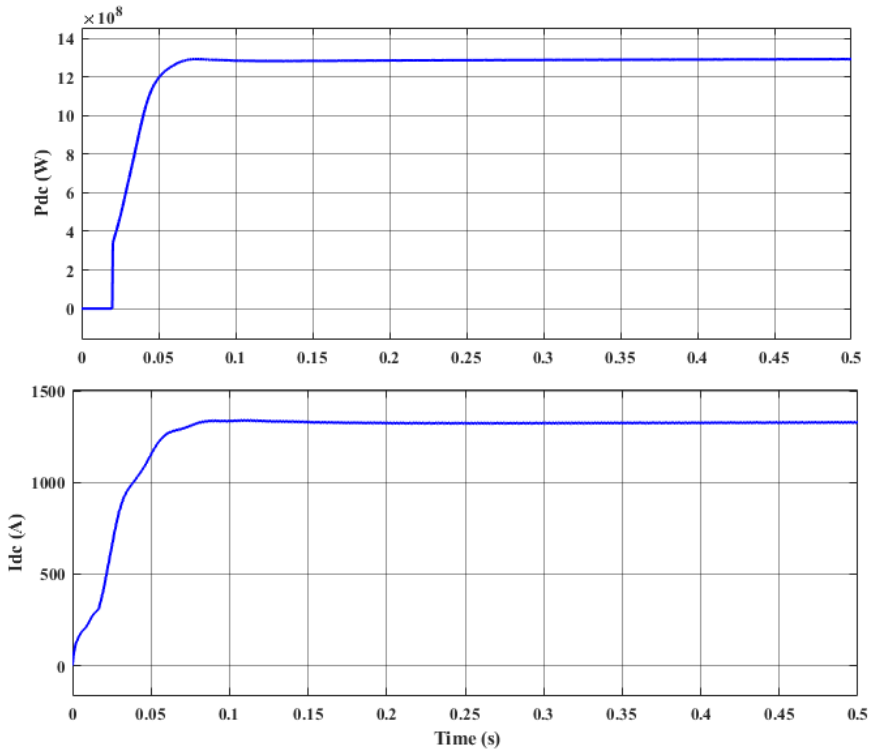

Figure 10 The output DC power and current at α=20 degree

.

C. Case II — PV transient: sudden irradiance drop (1000 → 500 W/m² at t = 0.5 s)

To assess the dynamic response of the PV system under realistic environmental fluctuations, a sudden drop in solar irradiance was introduced at 0.5 seconds, decreasing sharply from 1000 W/m² to 500 W/m². This abrupt transition emulates transient atmospheric conditions such as partial cloud coverage. Despite maintaining constant converter control angles—specifically a firing angle (α) of 25° and an extinction angle (γ) of 155°—the system experienced a noticeable dip in output active power and a corresponding modulation in voltage and current waveforms. The results, as depicted in Figure 11, clearly demonstrate the system's sensitivity to irradiance variations and its capability to stabilize after a short transient period, confirming the robustness of the control strategy under variable generation conditions.

This figure presents the output electrical parameters of the simulated PV farm. It shows the three-phase output voltage (Vabc) with a clear sinusoidal shape and stable amplitude, indicating correct synchronization with the grid and proper operation of the power electronic interface. The middle subplot presents the corresponding output current (Iabc), which is also sinusoidal and balanced to grid side. This validates the effective implementation of PV arrays and converters in controlling output waveforms. The bottom subplot illustrates the active power (P) output of the PV. Initially, the power ramps up to a peak of around 800 kW, followed by a brief drop due to irradiation fluctuation, and then stabilizes around 750 kW. This behavior confirms realistic generation and successful modeling response.

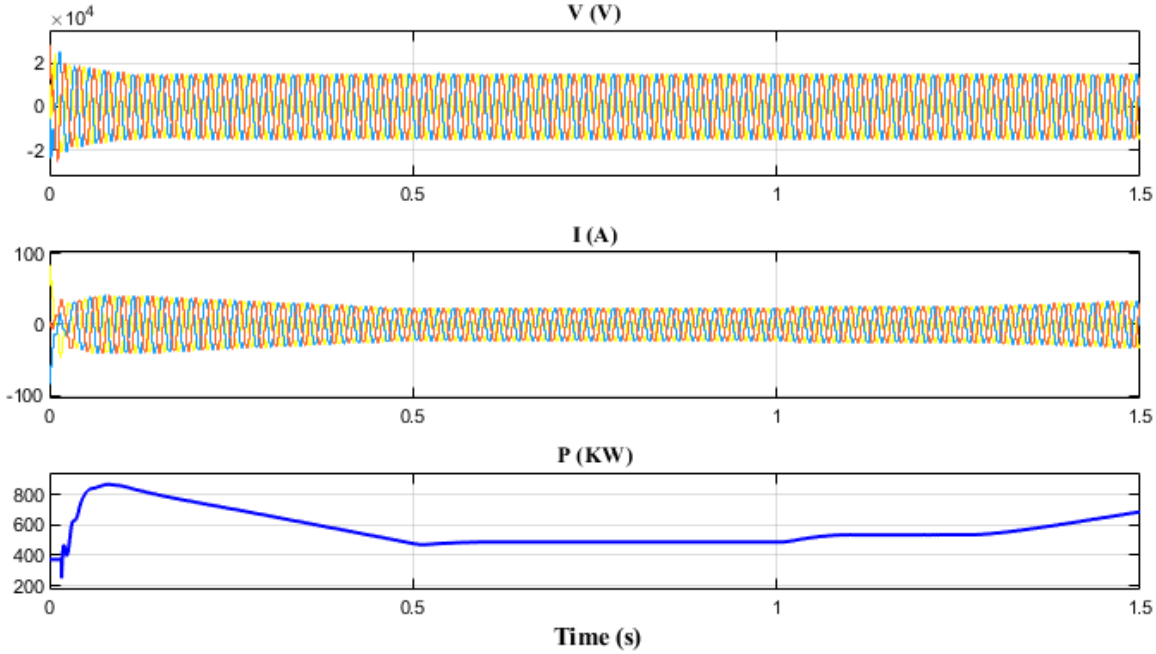

Figure 11 The voltage , current and power of the PV system with sudden change.

D. Case III — Firing & extinction angle variation (α and γ control)

To evaluate the influence of converter control on power transfer dynamics, a controlled variation of the rectifier station's firing angle (α) was performed while maintaining a constant solar irradiance of 1000 W/m² Specifically, the firing angle was increased from 25° to 40° and the extinction angle (γ) from 155° back to 120°. at a defined moment to emulate a power regulation or protection response. As illustrated in Figure [10], this alteration had measurable decrease in the transmitted active power was observed, which aligns with the theoretical behavior of LCC converters, where the output DC voltage is inversely related to the cosine of the firing angle. Consequently, the DC current through the HVDC link increased as α increased, leading to a proportional drop in power transfer at the rectifier station, as evidenced in figure 12. Notably, the DC voltages at both rectifier and inverter ends remained stable due to the controlled operation of the LCC and

the use of smoothing reactors. This case highlights the critical role of α in power modulation and demonstrates the system's ability to regulate output power electronically without impacting voltage quality.

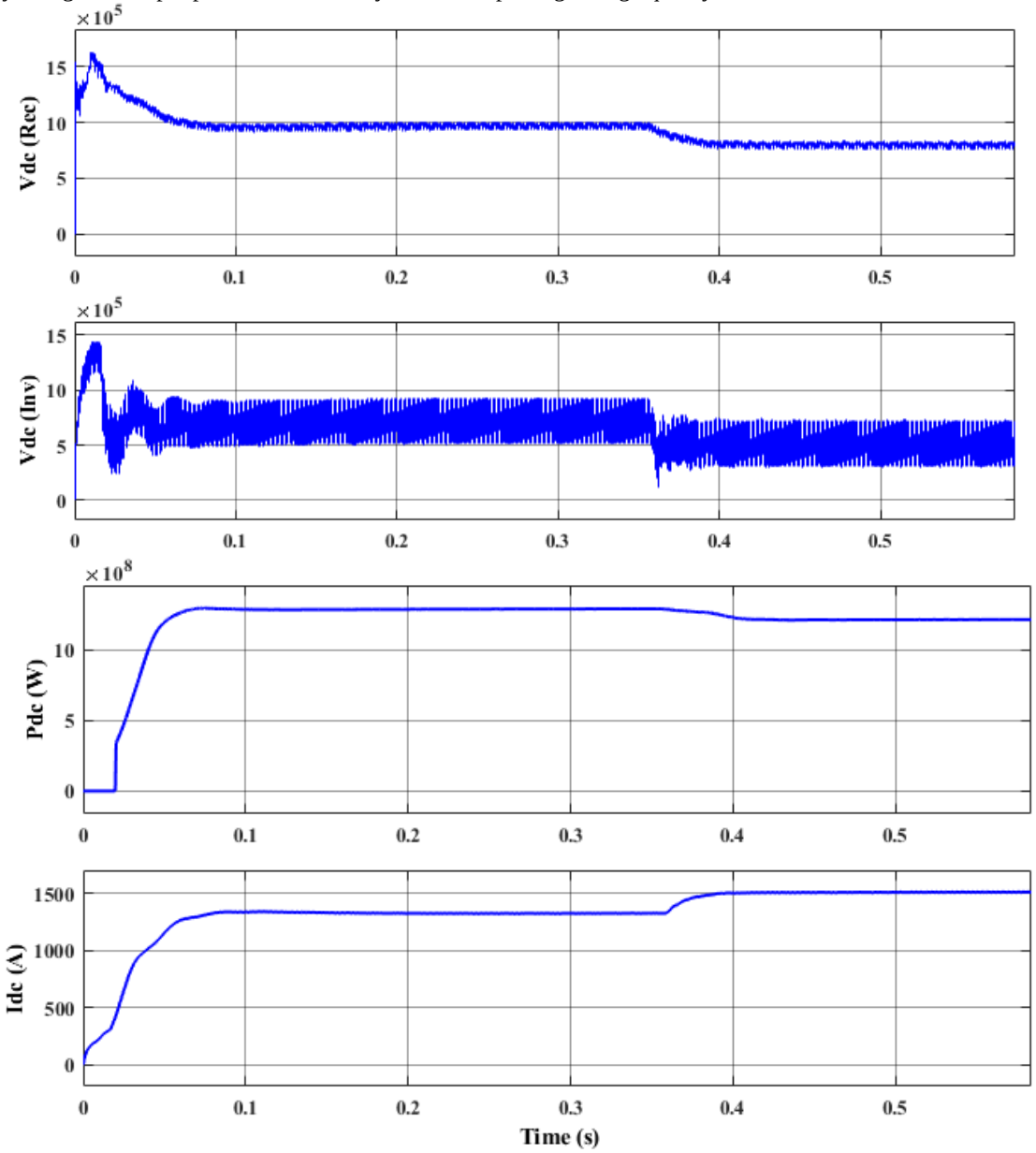

Figure 12 DC voltage output at rectifier and inverter station and transmitted power and current at firing angle alpha = 40 and gamma =120 degree.

E. Case IV — Voltage distortion due to commutation overlap (overlap angles / bulk converter effects)

The observed voltage distortion on both the rectifier and inverter sides can be attributed primarily to two key factors: the commutation (or overlap) angle and the scale of the converter station. In an LCC-HVDC system, when the firing angle (α) and extinction angle (γ) are set such that there is significant overlap between incoming and outgoing thyristors during each commutation event, the result is a non-ideal voltage waveform characterized by notches and flattened peaks. This overlap

causes a temporary short circuit between transformer windings, reducing the instantaneous output voltage and introducing harmonics into the AC waveform.

Moreover, the use of a large-scale bulk converter station—necessary for high-voltage and high-power handling—amplifies these effects due to the high current levels and the complex interaction of multiple six-pulse bridges in a twelve-pulse configuration. The distortion becomes more pronounced if the AC filters are under-designed or not finely tuned, especially when supplying power to weak grids. The result is a visibly deformed voltage waveform at both terminals, as evident in figure 13, with harmonic content mainly in the 5th, 7th, 11th, and 13th orders. This highlights the need for optimized commutation control and precise filter design to maintain voltage quality in high-power HVDC applications

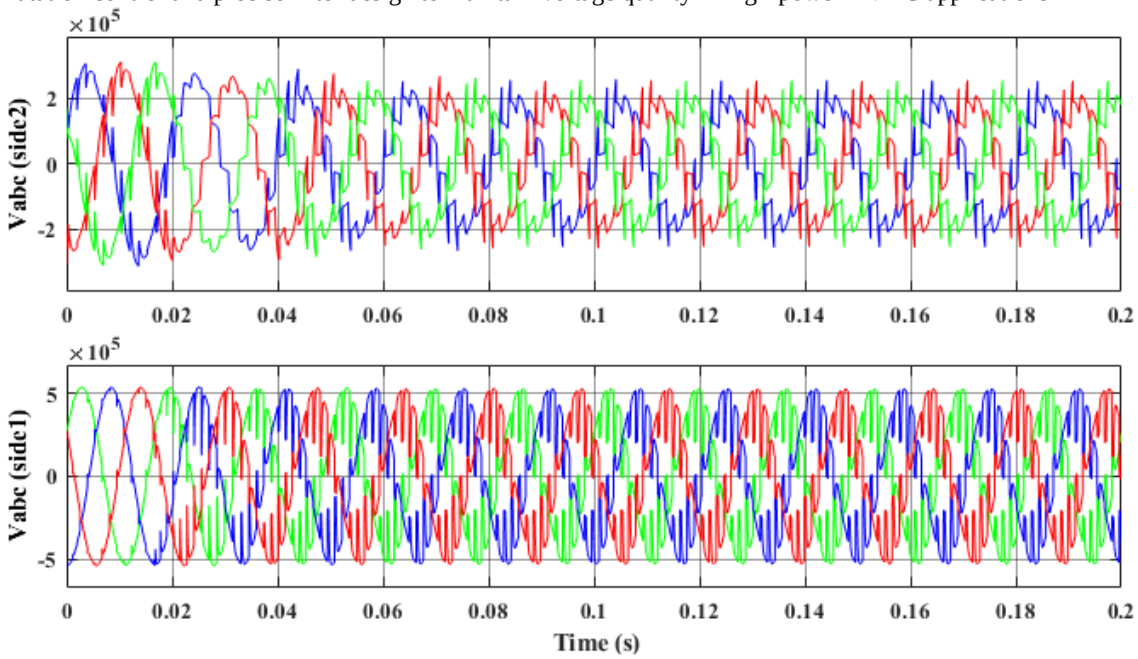

Figure 13 Distorted AC voltage at both sides without Passive filters .

F. Case V — Harmonic analysis (unfiltered) — FFT & THD report

When performing a Fast Fourier Transform (FFT) analysis of the voltage waveform at the rectifier station without employing any harmonic filtering, the Total Harmonic Distortion (THD) was observed to increase significantly, reaching 13.94% as depicted in figure 14. This level of distortion far exceeds the acceptable limits for power quality standards, such as those defined by IEEE Std. 519, which typically recommend that THD at the point of common coupling should not exceed 5% for voltages below 69 kV, and even less for higher transmission levels.

The elevated THD is a direct consequence of the line-commutated converter's operation, where the switching of thyristors during each cycle introduces characteristic harmonics—primarily the 5th, 7th, 11th, and 13th orders in a 12-pulse system. Without passive filters or advanced harmonic mitigation strategies, these harmonics remain embedded in the voltage waveform and propagate into the grid, leading to power quality issues, increased losses, overheating in transformers and rotating machines, and potential malfunction of sensitive equipment.

This result strongly emphasizes the necessity of incorporating well-designed passive filters at the converter station to suppress dominant harmonics and maintain compliance with grid code requirements.

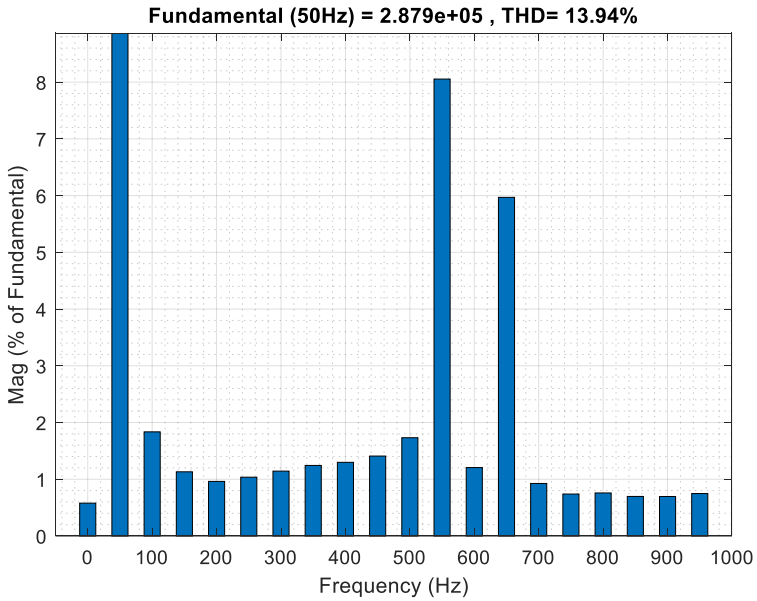

Figure 14 harmonic voltage signal spectrum at rectifier side.

G. Case VI — Harmonic mitigation with passive filters (post-filter results)

After implementing passive filters at both the rectifier and inverter sides, the AC voltage waveforms were significantly improved, exhibiting nearly ideal sinusoidal shapes as illustrated in figure 15. This enhancement is due to the effective attenuation of characteristic harmonics, particularly the 5th, 7th, 11th, and 13th, which are typically introduced by the 12-pulse converter operation. The passive filters, designed to target these dominant harmonics, successfully minimized voltage distortion and reduced the Total Harmonic Distortion (THD) to within acceptable standards 0.93% as depicted in figure 16. As a result, the voltage quality at both terminals of the HVDC system was restored, ensuring compliance with grid code requirements and improving overall system performance

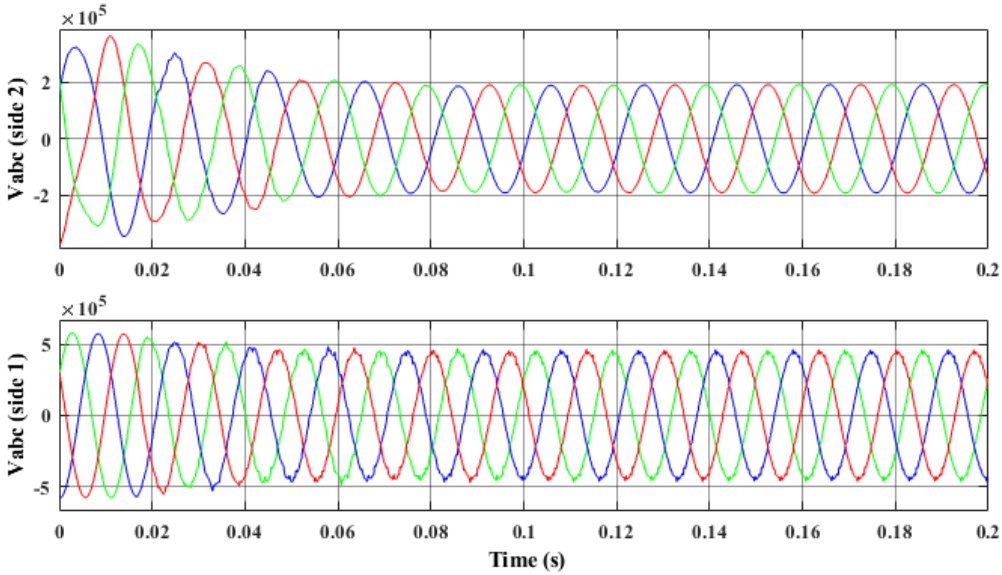

Figure 15 improved AC voltage at both sides after adding Passive filters .

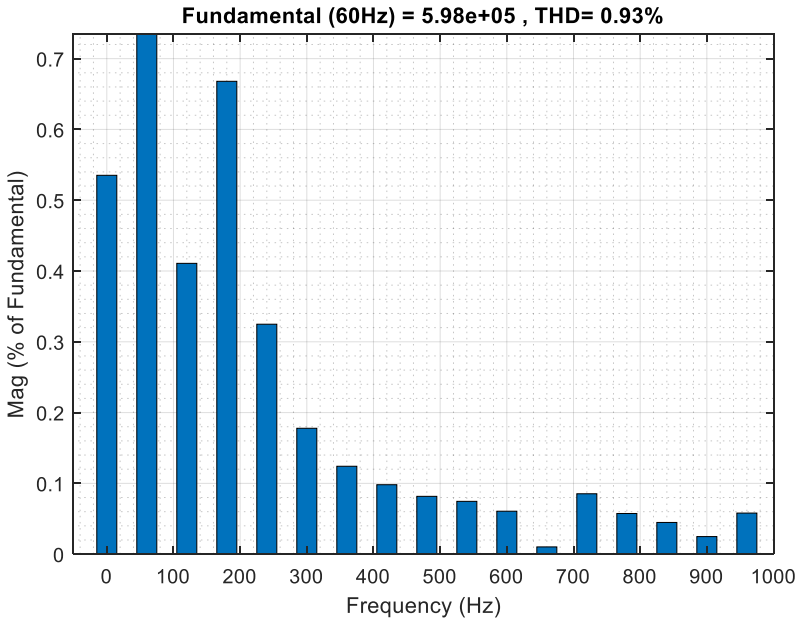

Figure 16 harmonic voltage signal spectrum at rectifier side.

IV. Conclusion

This research successfully developed and analyzed a comprehensive simulation model for a hybrid photovoltaic generation system interconnected via a bipolar LCC-HVDC transmission link. The proposed configuration effectively supports large-scale renewable integration by ensuring efficient power delivery over long distances while addressing the key challenges of harmonic distortion and reactive power compensation.

Through various dynamic simulations, it was observed that firing angle modulation directly influences transmitted power, while solar irradiance variations cause significant impacts on current and voltage stability. Moreover, the implementation of passive filters at converter stations markedly reduced the Total Harmonic Distortion (THD) from 13.94% to 0.93%, restoring voltage waveforms to near-perfect sinusoidal profiles.

The findings confirm the technical feasibility and operational advantages of integrating large-scale PV systems through LCC-HVDC infrastructure, emphasizing the importance of coordinated control and filter design in maintaining system stability and grid compliance. The proposed model serves as a valuable reference for future renewable-HVDC integration projects.

REFERENCES

[1] S.M. Muyeen, H. Senjyu, H. Fujita, Recent advances in integration of renewable energy with power grid, Energies 12 (2019) 2955. https://doi.org/10.3390/en12152955.

[2] J.P. Barton, D.G. Infield, Energy storage and its use with intermittent renewable energy, IEEE Trans. Energy Conversion 19 (2020) 441–448. https://doi.org/10.1109/TEC.2020.2998419.

[3] K. Wang, Z. Xu, Y. Zhang, Y. Song, Dynamic performance analysis of renewable energy integrated HVDC systems, IEEE Trans. Power Delivery 36 (2021) 1850–1859. https://doi.org/10.1109/TPWRD.2020.3039134.

[4] A. Mehrizi-Sani, R. Iravani, Distribution system operation with distributed energy resources: A review of drivers, challenges, and opportunities, IEEE Trans. Smart Grid 11 (2020) 3274–3286. https://doi.org/10.1109/TSG.2019.2951441.

[5] S. Sakamuri, R.K. Varma, S. Pannu, HVDC transmission for enabling renewable energy corridors in developing

countries, IEEE Access 8 (2020) 219523–219537. https://doi.org/10.1109/ACCESS.2020.3042381

[6] L. Zhang, L. Harnefors, H.-P. Nee, Control of HVDC transmission systems under renewable power variability, IEEE Trans. Power Electronics 35 (2020) 3982–3994. https://doi.org/10.1109/TPEL.2019.2934169.

[7] Ministry of Electricity and Renewable Energy of Egypt, Egypt–Saudi Arabia HVDC Interconnection Project: Strategic Overview, White Paper (2021). [No DOI available]

[8] M.S. El Moursi, A. Al-Shetwi, H.H. Zeineldin, Y. Atwa, Advanced control and protection of HVDC grids: A review, IEEE Access 8 (2020) 211236–211256. https://doi.org/10.1109/ACCESS.2020.3039043.

[9] L. Tang, B.T. Ooi, Protection of DC lines in hybrid HVDC systems, IEEE Trans. Power Delivery 35 (2020) 292–300. https://doi.org/10.1109/TPWRD.2019.2938023.

[10] C.U. Ogbuka, C.O. Okoye, E. Agwu, Review of HVDC control methods for renewable integration, Renew. Sustain. Energy Rev. 136 (2021) 110431. https://doi.org/10.1016/j.rser.2020.110431.

[11] Younis, R. A., Ibrahim, D. K., Aboul-Zahab, E. M., & El Gharably, A. F. (2020). Techno-economic investigation using several metaheuristic algorithms for optimal sizing of stand-alone microgrid incorporating hybrid renewable energy sources and hybrid energy storage system. *International Journal on Energy Conversion*, *8*(4), 141-152.

[12] K. Alqunun *et al*., "Advancements in Hybrid Energy Storage Systems for Rural Electrification: A Comprehensive Case Study on Siwa Oasis in Egypt on Increasing Battery Longevity in Standalone PV Systems," in *IEEE Access*, vol. 13, pp. 85239-85259, 2025, doi: 10.1109/ACCESS.2025.3569644.

[13] R. A. Younis, R. A. Abdelrahman, N. M. Mansour and A. A. Salem, "Modeling and Performance Evaluation of a Hybrid PV/Wind/Diesel Generation Units Under Certain Operating Conditions," *2023 24th International Middle East Power System Conference (MEPCON)*, Mansoura, Egypt, 2023, pp. 1-7, doi: 10.1109/MEPCON58725.2023.10462258.

[14] Y. Shi, Z. Cao, Y. Wu, Multi-objective optimal design of AC filters in HVDC systems using enhanced MOEA/D, *High Voltage* (Wiley) 8 (2023) 123–134. https://doi.org/10.1049/hve2.12291.

[15] K. Zhai, D. Zhao, Y. Xue, Filtering characteristics of parallel-connected fixed capacitors in LCC-HVDC considering system strength variations, *Frontiers in Energy Research* 12 (2024) 1370585. https://doi.org/10.3389/fenrg.2024.1370585.

[15] Y. Jin, L. Ye, Y. Zhao, W. Chen, Y. Han, Y. Su, "Adaptability Analysis of Asynchronous Interconnected LCC-HVDC with Additional Frequency Control Strategy," in Proceedings of the 7th Purple Mountain Forum on Smart Grid Protection and Control (PMF2022), Springer, Singapore, pp. 195–206, 2023. https://doi.org/10.1007/978-981-99-0062-6_14 SpringerLink

[16] P. Peihong, X. Xiaoyong, H. Hui, S. Xizhi, Z. Zilei, C. Chunming, L. Lianguang, "Modelling and analysis of LCC-HVDC converter station for harmonic coupling of AC/DC power grid during geomagnetic storm," IET Power Electronics, vol. 16, no. 14, pp. [to be filled], Nov. 2023. https://doi.org/10.1049/pel2.12565

[17] H. Wang, W. Wang, "MMC-HVDC High-Frequency Resonance Suppression Strategy Based on Multi-Band Band-Stop Filters," Sustainability, vol. 15, no. 18, p. 13309, 2023. https://doi.org/10.3390/su151813309

[18] H. Li, Y. Li, Y. Meng, K. Yan, "Coordinated frequency support strategy for VSC-HVDC integrated offshore wind farm system," Frontiers in Energy Research, vol. 12, Feb. 2024. https://doi.org/10.3389/fenrg.2024.1351353

[19] Q. Wang, Z. Li, A. Luo, X. Yang, "Simulation Study on Operation Characteristics of Multi-terminal Flexible HVDC Transmission System Based on Wind Power and Photovoltaics," in Proc. 18th Annual Conference of China Electrotechnical Society (ACCES 2023), Lecture Notes in Electrical Engineering, vol. 1165, pp. 425–432, 2024. https://doi.org/10.1007/978-981-97-1351-6_46

[20] R. Shaheer Mehmood, A. Hussain, U. Ali, M. T. Mahmood, "Novel Double-Damped Tuned AC Filters in HVDC Systems," Computers, Materials & Continua, vol. 77, no. 1, pp. 1467-1482, 2023. https://doi.org/10.32604/cmc.2023.033280

[21] Y. Liu, C. Shen, Z. Wang, "Distributed Emergency Frequency Control Considering Transient Stability Constraints in Multi-Infeed Hybrid AC-DC System," arXiv preprint arXiv:2210.07497, 2022. https://doi.org/10.48550/arXiv.2210.07497

[22] "Review of HVDC technologies for weak grid interconnectors," Electrical Engineering, vol. 107, pp. 4483-4501, 2025. Springer. https://doi.org/10.1007/s00202-024-02761-6